Phase coherence between cardiovascular oscillations in malaria: the basis for a possible diagnostic test

Y. A. Abdulhameed[1], A. G. Habib[2], P. V. E. McClintock[3], and A. Stefanovska[4]

[1] Department of Physics, Lancaster University, Lancaster LA1 4YB, United Kingdom y.abdussalam@lancaster.ac.uk
[2] Department of Medicine, Bayero University, Kano, Nigeria abdulrazaq_habib@yahoo.co.uk
[3] Department of Physics, Lancaster University, Lancaster LA1 4YB, United Kingdom p.v.e.mcclintock@lancaster.ac.uk
[4] Department of Physics, Lancaster University, Lancaster LA1 4YB, United Kingdom aneta@lancaster.ac.uk

Summary. We show how a non-autonomous dynamics approach using time-resolved analyses of power spectra and phase coherence can help in the noninvasive diagnosis of malaria. The work is based on studying oscillations in blood flow and the variability of the heart and respiratory frequencies. The model used assumes that the heart and respiration are two oscillatory pumps with variable frequencies and that the vascular resistance also changes in an oscillatory manner. Red blood cells circulating through the system deliver oxygen to each cell. Malaria changes the red blood cells so that this delivery is compromised. The oscillatory properties of both pumps are also affected. We quantify the latter and compare three groups of subjects: febrile malaria patients (37); non-febrile malaria patients (10); and healthy controls (51). For each subject, time series of skin blood flow, respiratory effort, cardiac activity (ECG) and skin temperature were recorded simultaneously over an interval of 30 minutes. The oscillatory components within the range $0.005 - 2\,\mathrm{Hz}$ were analysed and their degree of coordination throughout the cardiovascular system was assessed by wavelet phase coherence analysis. It is shown that malaria, either febrile or non-febrile, substantially reduces the coordination.

1 Introduction

Malaria is a life-threatening mosquito-borne disease [41], involving changes in the dynamical properties of blood flow. There are still more than 200 million cases of malaria annually, resulting in 600,000 deaths. The disease is treatable when arrested soon enough, so early diagnosis is highly desirable. Despite the development of non-invasive alternatives [22], the current gold standards in malaria diagnosis are still

antigen-based rapid diagnostic tests (RDTs) and the microscopic examination of blood films by a trained microscopist. Results vary widely in diagnostic sensitivity and specificity.

To our knowledge, malaria-related impairment of cardiovascular oscillation has not been investigated. To try to understand such effects, and to assess their potential for detecting malaria, the present study involves simultaneous monitoring of blood flow, skin temperature, respiration and electrocardiography. The time series are analysed using wavelet-based methods to establish, not only the intensity of oscillatory processes involved in cardiovascular regulation, but also their degree of coordination which, as we will see, is adversely affected by malaria.

Physiological oscillations and their potential for characterising cardiovascular dynamics in malaria. Measurements of blood flow and oxygenation in human subjects reveal several co-existing oscillatory processes, covering a very wide range of frequencies. Use of the continuous wavelet transform reveals at least six such processes [34, 36]; with the same oscillations being seen at different sites and for different measured quantities, not only in blood flow and oxygenation. Their physiological attribution has been established. Briefly: hemodynamic oscillations near 1 Hz (frequency interval FI-I) and 0.25 Hz (FI-II) are due to cardiac and respiratory activity respectively; the oscillation near 0.1 Hz (FI-III) is attributable to the natural properties of smooth muscle which oscillates at about 0.1 Hz even *in vitro*; that near 0.03 Hz (FI-IV) is neurogenic, associated with autonomic nervous activity; and those near 0.01 Hz (FI-V) and 0.007 Hz (FI-VI) arise [23] from NO-related and NO-independent endothelial activities respectively. The underlying physiological oscillatory processes suggested the introduction of a coupled-oscillator model of the cardiovascular system [36, 37, 39]. Understanding the nature of these oscillations in healthy subjects allows their sometimes distinctive differences in pathological states to be identified. This approach has not yet been applied to malaria, however, even though the disease may be expected to cause significant changes in microvascular dynamics.

Possible effects of malaria on the oscillations in blood flow. The increased stiffness of the membrane of an infected erythrocyte (red blood cell, or RBC) [19], and its tendency to stick to the endothelial cells lining all the blood vessels, cause infected cells to pass less easily through the capillaries. The cell also changes shape, and its ability to transport/release oxygen is compromised. Consequently, the viscosity, flow properties, and oxygenation of blood are all changed by malaria in ways that do not occur in other diseases. Hemodynamics is altered [18] on account of the spatial distribution of erythrocytes [33] and merozoites, and it is reasonable to infer that endothelial reactivity is affected too. Erythrocytes are an important factor determining the hemorheological properties of blood its corresponding shear-thinning and increased shear stress at walls [46]. We therefore hypothesise that the oscillatory properties and their degree of coherence between different parts of the system will be altered in malaria. Blood flow takes place in a thermodynamically open system, and therefore the oscillations are time-varying. Time series analysis methods for non-autonomous dynamics [8, 9]must therefore be employed.

Table 1. Anthropometric data for the subjects, presenting their: ages; body mass index (BMI); skin temperature (ST); core temperature (CT); instantaneous heart rate (IHR); instantaneous respiration rate (IRR); systolic blood pressure (SBP); diastolic blood pressure (DBP); and blood packed cell volume (PCV). Median values and their ranges (25th and 75th percentiles) are shown, with significant differences ($p < 0.05$) highlighted in grey. $p1$, $p2$ and $p3$ are values obtained from the sign rank test for FM-NFM, FM-NM and NFM-NM comparisons respectively.

	FM ($n = 37$)	NFM ($n = 10$)	NM ($n = 52$)	$p1$	$p2$	$p3$
Age (years)	20(18-25)	23(20-27)	22(20-24)	0.08	0.169	0.382
BMI (kg/m^2)	19.8 18.1-21.8	20 19.5-21.5	21.1 19.1-22	0.53	0.058	0.6
ST (^{o}C)	38.2 37.6-38.9	35.5 35.1-36.4	35.9 35.7-36.1	2×10^{-6}	10^{-9}	0.514
CT (^{o}C)	38.9 38.2-39.2	37.80 37.6-38.0	36.15 35.9-36.5	10^{-9}	2×10^{-5}	7×10^{-5}
IHR (Hz)	1.72 1.53-1.85	1.36 1.28-1.55	1.14 1.02-1.26	0.002	0.00009	0.00009
IRR (Hz)	0.44 0.37-0.49	0.35 0.32-0.45	0.33 0.30-0.37	0.02	3×10^{-7}	0.325
SBP (mm Hg)	112 106-125	113 106-118	124 110-128	0.79	0.039	0.07
DBP (mm Hg)	63 57-70	73 68-80	77 69-82	0.03	0.00014	0.45
PCV (%)	42 40-43	44 41-45	44 42-47	1	0.02	0.17

2 Materials and Methods

Here we summarise salient features of the measurements and data analysis, which are described in fuller detail by Abdulhameed [1]. The anthropomorphic data for the subjects used in the study are listed in Table 1.

2.1 Subjects and plan of the study

Consecutive adult male patients presenting to Murtala Mohammed Specialist Hospital, Kano, Nigeria with acute ailments and fever during August–November 2017 were evaluated by taking clinical history and examination. Blood samples for tests were collected from patients considered likely to have malaria for subsequent malarial smear microscopy, rapid diagnostic tests (RDT), haematocrit level and for haemoglobin genotype. These tests were conducted later but the physical data acquisition was conducted immediately in a cool and quiet place as detailed in subsection 2.2 on patients considered

likely to have malaria. Where the results of the medical tests subsequently confirmed presence of malaria, absence of anaemia (low haematocrit) and AA genotype, patients were retained in the study and categorized as febrile malaria (FM) (37) or non-febrile malaria (NFM) (10). The results of 20 patients who did not fit the criteria were discarded, regardless of malarial status, because anaemia and or abnormal haemoglobin genotype are known to affect blood flow dynamics and RBC morphology and consequently the physical parameters being studied. A control group of 51 healthy non-malaria (NM) male subjects was also recruited.

For all subjects, the inclusion criteria included: (i) informed consent for participation in the study, under a protocol approved by the Ethical Committees of both the Kano State Ministry of Health, Nigeria and Bayero University Kano, Nigeria; (ii) absence of overt alternative/superadded cause of febrile illness; (iii) absence of significant co-morbidity/complications known to affect the test, e.g. hypertension or peripheral vascular disease; (iv) absence of sickle cell anaemia in a blood group genotype test; and (v) having the AA genotype blood group.

For the FM and NFM groups, additional inclusion criteria were: (vi) presence of malarial parasites in blood film microscopy; and (vii) a positive malarial Rapid Diagnostic Test (RDT). The difference in the inclusion criteria for febrile malaria and non-febrile malaria group was body temperature. Malaria patients presenting with a core temperature above 38.0^{o}C were defined as FM, while those with lower temperatures were defined as NFM.

For the NM group, the additional inclusion criteria were: (vi) no acute febrile illness (temperature $< 36.0^{o}$C); (vii) absence of malarial parasites in blood film microscopy; and (viii) a negative malarial RDT.

In the FM group, 30% of the patients had taken antimalarial and antipyretic drugs before presenting; 40% had taken antipyretic drugs only, and 30% had not taken any drugs. In the NFM group, all patients had taken antimalarial and/or antipyretic drugs for at most 3 days.

2.2 Data acquisition

The measurements were all made between 09:00 and 18:00 in a quiet air-conditioned room, with a controlled ambient temperature and constant low illumination.

Microvascular blood flow was recorded by laser-Doppler flowmetry (LDF), which provided a continuous measurement of the microcirculation in the skin, thus reflecting the perfusion in the capillaries, arterioles, venules and dermal vascular plexus. The instrument (moorLAB, Moor Instruments Ltd, UK) used in the present study transmits a near-IR laser light from a temperature-stabilized laser diode operating at a wavelength of 780 nm and with a maximum power of 2.5 mW into the skin through an MP1-V2 probe (Moor Instruments Ltd, UK), which has two optical fibres. A time constant of 0.1 s was selected and the LDF processor bandwidth was between 18 Hz and 22.5 KHz.

A flexible probe holder (PH1-V2, Moor Instruments Ltd., UK) was attached to the skin surface on the outer side of each ankle (lateral malleolus) using double-sided adhesive discs. One fibre delivers light to the site under observation, while the backscattered (reflected) light is collected by the other fibre. The light reflected back from moving RBCs is Doppler-shifted in frequency by an amount related to the blood flow in the illuminated volume of tissue, the frequency shift being proportional to red cell speed, while the frequency of the light reflected from stationary cells and tissue remains unchanged [29]. The difference between incident light and the Doppler-shifted back-scattered light yields the LDF signal, known as the blood perfusion signal. The LDF output is semi-quantitative and is expressed in perfusion units (PU) of output voltage (typically 1 PU = 10 mV) [29]. The sampling frequency was 40 Hz.

An electrocardiogram (ECG) was used to record the electrical activity of the heart with a sampling frequency of 1 kHz. The ECG was measured using a bipolar precordial lead. The electrodes were attached on both shoulders and the lowest left rib, as this maximizes the sharpness of the R-peak.

The respiration was measured using an elasticated belt fastened across the chest and fitted with a Biopac TSD201 Respiratory Effort Transducer (Biopac Systems Inc., CA, USA).

Skin temperature was monitored using two high-sensitivity, low-heat-capacity thermistors – YSI 709B Thermilinear sensors (YSI Inc, Yellow Springs, OH, USA) of 8.5 mm diameter, which were taped onto the skin. The thermistors were positioned outside the left ankles, over the lateral malleolus, close to the LDF probes.

The individual time series were recorded simultaneously using a signal conditioning system (Cardiosignals, Institute Jožef Stefan, Slovenia) over an interval of 30 minutes.

Blood pressure was measured prior to the initiation of signal acquisition. A Digital Automatic Blood Pressure Monitor (Omron, M10-IT) was used, with a cuff wrapped on the subjects' upper right arm while they were seated. The subject then moved to a supine position on a comfortable bed, where the necessary sensors were installed. In this way, subjects relaxed in a supine position for 15–20 min of acclimatisation, prior to the recordings. The equipment was either battery supplied or connected to the electrical supply via a mains filter.

3 Analysis of cardiovascular time series

Prior to analysis, time-series were inspected in order to detect any apparent anomalies, e.g. movement artefacts or rhythmic patterns clearly different from the blood flow oscillations of interest. Most often, these effects stemmed from methodological or physiological factors including poor electrode placement or poor contact due e.g. to dry skin. Time series that were demonstrably defective were discarded.

3.1 Spectral analysis

Traditionally, representations of time series in the frequency domain are obtained with the fast Fourier transform, which constitutes a periodic function in terms of sines and cosines. This makes it suitable for analysing time series whose components are strictly periodic in nature, but it is unsuitable for LDF blood flow signals whose spectral content is inherently non-periodic. Although the limitations of the Fourier transform can partially be addressed by dividing the time series into shorter time-windows within which there is not much time variation, a better way forward is by the use of wavelet analysis [38] which, by using an adaptive window length that simultaneously analyses time series at each moment in time, provides both optimal frequency resolution and time localisation [8, 14].

Wavelet analysis is a scale-independent method comprising an adaptive window length allowing low frequencies to be analysed using longer wavelets, and higher frequencies with shorter wavelets. The continuous wavelet transform $W_s(s,t)$ of a signal $f(t)$ is defined as

$$W_s(s,t) = |s|^{-1/2} \int_{-\infty}^{\infty} \psi\Big(\frac{u-t}{s}\Big) f(u) du, \tag{1}$$

where s is the scaling factor, t is the temporal position on the signal, and the wavelet function is built by scaling and translating a chosen mother wavelet ψ which, in this study, was chosen to be the complex Morlet wavelet, equation (2), because it maximizes joint time-localisation and frequency-resolution [38]

$$\psi(u) = \frac{1}{\sqrt{\pi}} \big(e^{-i\omega_0 u} - e^{-{\omega_0}^2/2}\big) e^{-u^2/2}. \tag{2}$$

3.2 Extracting the instantaneous heart frequency

The instantaneous heart rate (IHR) was extracted from the data using both time-frequency and time domain analysis techniques [16]. The methods used included nonlinear mode decomposition (NMD) [17], a technique that decomposes a signal into a set of components, or modes. Using NMD, the instantaneous frequency of the heart beat was extracted from the wavelet transform of the ECG, thus yielding the IHR. The IHR was also derived from the LDF signals using the same technique. Note that in the literature [15, 26] IHR is often referred to as HRV and, occasionally, as IHF.

3.3 Wavelet phase coherence

While waves can be coherent in space, oscillations can be coherent in time. Quite generally, correlation properties between physical quantities, whether at a single or several oscillation frequencies, can be studied by investigating their coherence in time. If we observe oscillations at the same frequency in two

different time series and find that the difference between their instantaneous phases $\phi_{1k,n}$ and $\phi_{2k,n}$ is constant, then the oscillations are said to be coherent at that frequency [3,5,32]. A phenomenon closely related to coherence is that of phase synchronization [13,20,28,30]. While oscillations can be coherent without necessarily being directly coupled, the existence of coupling is fundamental for synchronization [8]. For example, if we have an n:m relationship between the frequencies of two signals, this implies that there are n oscillation cycles in one time series per m cycles of the other time series: 1:1 phase synchronization may equally be considered as phase coherent oscillations. Thus phase coherence can be used directly to investigate 1:1 synchronization between two signals, such as the blood flow and oxygen saturation signals used in the present study. The wavelet phase coherence (WPC) $\gamma(f)$ between the two signals $f_1(t)$ and $f_2(t)$ is estimated from their respective wavelet transforms as obtained in equation (1), i.e. $W_{s_{1,2}}(t,f)$ [38] as

$$\gamma(f) = \left| \frac{1}{T} \int_0^T e^{i \arg[W_{s_1}(s,t) W^*_{s_2}(s,t)]} dt \right| \tag{3}$$

where T is the duration of the signal. This equation reflects the extent to which the phases $\phi_{1k,n}$ and $\phi_{2k,n}$ of both signals at each time t_n and frequency f are entirely correlated. Unlike the usual coherence measures, wavelet phase coherence takes no account of the amplitude dynamics of the signals. This is appropriate because (i) the amplitudes of most physiological signals are subject to artefacts and noise, and (ii) the relationships between the amplitudes of common physiological oscillations can be complicated and nonlinear. In all cases, however, the relationship between their phases remains the same (up to a constant phase shift). Their relative phase difference is thus calculated as

$$\Delta\phi_{kn} = \phi_{2k,n} - \phi_{1k,n} \,. \tag{4}$$

The phase coherence function $C_\phi(f_k)$ is obtained by calculating and averaging in time the components of the sine and cosine of the phase differences for the whole signal, effectively defining the time-averaged WPC as

$$C_\phi(f_k) = \sqrt{\langle \cos \Delta\phi_{kn} \rangle^2 + \langle \sin \Delta\phi_{kn} \rangle^2}. \tag{5}$$

The idea behind equation (3) is that, while we are considering individual times and frequencies, these come from a discrete set (since all the signals in the present study are discrete and finite-time), and so the subscripts k and n just reflect this discreteness. The phase coherence function $C_\phi(f_k)$ as defined in equation (5) is exactly the discrete version of the phase coherence formula equation (3), where ϕ is the phase difference between the signals in question.

The function $C_\phi(f_k)$ characterises the tendency of $\Delta\phi_{kn}$ to remain constant, or not, at a certain frequency. Its value lies between 1 implying perfect coherence, and 0 implying total incoherence.

Effective (or significant) coherence

Note that the coherence computed in the first instance does not necessarily reflect a genuine phase relationship and requires careful evaluation. The problem arises because some of the coherence values obtained can be less than zero (although formally coherence values range between 0 and 1). These negative coherence values are then subtracted. Following this procedure, the very low frequency oscillations may appear to have a coherence values close to 1, because of bias resulting from the use of recordings that are too short to encompass the content at low frequencies.

Even in the case of two noisy signals, there is a tendency for there to be some apparent coherence in the sense that $C_\phi(f_k)$ rarely approaches 0 at very low frequencies. The degree of apparent phase coherence depends on frequency. So the coherence baseline will not be the same for all scales. The low-frequency components, particularly for signals of finite length (like ours) are evaluated using fewer periods than for the higher frequency components [5]. The result can be an artificially increased coherence $\simeq 1$ even where, in reality, the dynamics of the signals are completely unrelated.

To minimise random effects giving rise to apparent (but spurious) coherence, whether at low or high frequency, we checked/tested the significance of the computed coherence using the method of surrogates [24, 31] – by setting as a null hypothesis that, for all frequencies, the phases in the signals are independent. We used iterative amplitude-adjusted Fourier transform (IAAFT) surrogates to estimate the significance level of the apparent coherence, thereby avoiding the bias associated with the power spectrum of the more commonly used amplitude-adjusted Fourier transform (AAFT) surrogates. First, the IAAFT surrogates are constructed by randomizing all the properties of the signals in question, whilst keeping only the phases unshuffled. Subsequently, this is accomplished in an iterative fashion, simply by using the appropriate value and re-scaling the distribution to substitute Fourier amplitudes, which allows us to obtain resemblance between the distributions and power spectra of the surrogates and the original signals. At each frequency we took the coherence threshold to be 95% of the highest value of 100 random realisations of IAAFT surrogates.

Finally, the effective/significant coherence was estimated by subtracting the 95th percentile of the 100 surrogate values, thus yielding the extent to which the phases of the two signals at each frequency are correlated.

Statistical analysis

Non-parametric statistical tests were used, implying that no assumptions were being made about any underlying distributions, thus allowing robust conclusions to be drawn. The Wilcoxon rank sum test [43] was used to test for possibly significant differences between blood flow and other signals measured from malarial and control subjects, respectively, as the corresponding time-series do not match. The Wilcoxon rank sum test is used to determine whether two

unmatched samples come from similar distributions, whilst the sign rank test requires that the samples are matched. In all cases, $p < 0.05$ was considered as being statistically significant.

4 Results

4.1 Effect of malaria on blood pressure, respiration frequency, and skin temperature

As summarised in Table 1, the FM group differed from the NM group in all parameters, including skin and core temperatures, heart and respiratory rates, systolic and diastolic blood pressures, and blood packed cell volume. The NFM group, on the other hand, differed in some parameters but not in all. FM differed from NFM in all parameters except SBP and PCV. NFM differed from NM only in core temperature and IHR.

4.2 Detecting oscillations using time-frequency analysis

The signals were transformed to the time-frequency domain by wavelet analysis with a Morlet wavelet of $f_0 = 1.5$ Hz, using custom Matlab codes. The time-averaged power was then calculated and normalised in each case. Note that, even where the time-averaged values of two signals are the same, computation of their wavelet transforms can often reveal statistically significant differences. A similar scenario was observed in the subsequent analysis of cardiovascular dynamics in malaria and non-malarial states in some of the characteristic frequency intervals. The differences observed in power spectra between malaria states and non-malaria were further investigated in order to ascertain whether they could be used to distinguish between groups. To test the reliability of these parameters, machine learning algorithms were used to classify them between the FM, NFM and NM states. Whilst the evaluation of absolute wavelet spectra power is promising, it does not in itself reveal a sufficient difference in oscillatory energy, when compared between groups. Difficulties are often faced when characterizing and comparing oscillations in specific frequency intervals, on account of global differences in the spectral power between groups. All the wavelet power spectra were therefore normalized by dividing by their total powers; comparisons of the normalised power could then be made between groups at each of the characteristic frequencies within 0.005-2 Hz. However, we present both blood flow and instantaneous heart frequency in terms of their absolute power.

Spectral power in blood perfusion fluctuations

The normalized time-averaged wavelet powers of left (BF1) and right (BF2) blood flow oscillations for the three groups shown in Figure 1.

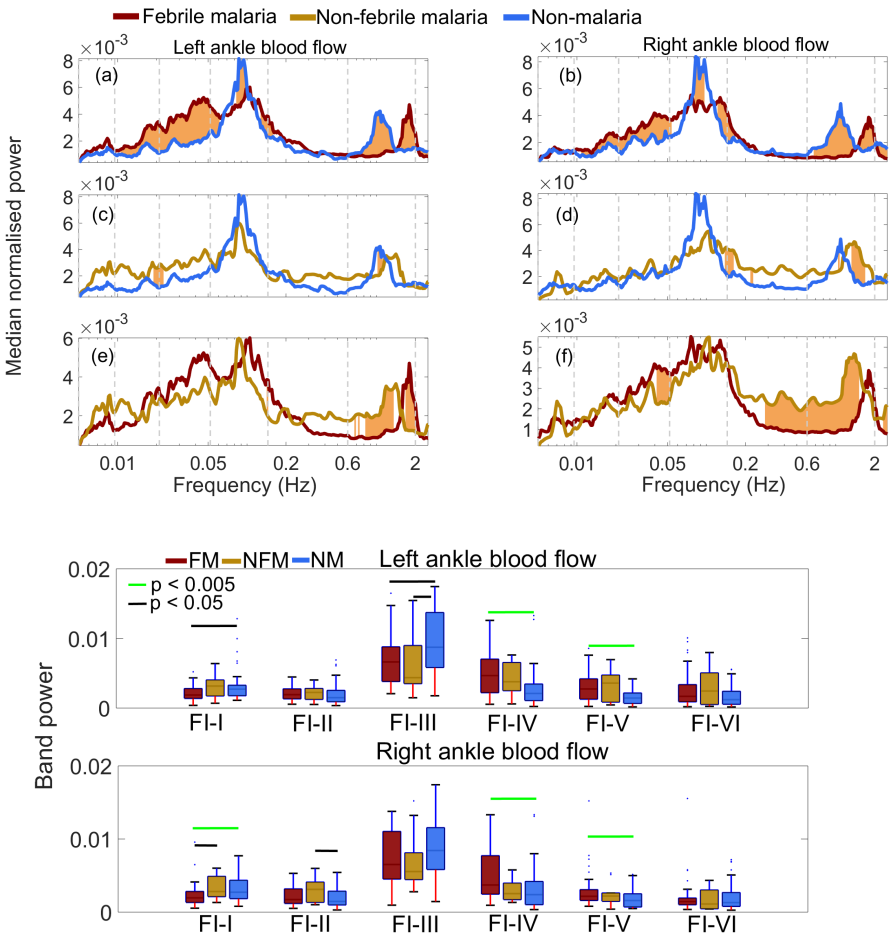

Fig. 1. Normalised wavelet power: (a)-(f) Normalised time-averaged wavelet power of left (first column) and right (second column) ankle blood flow for each group. Significant differences ($p < 0.05$)in pair comparisons are highlighted in brown. The frequency intervals FI–I... FI–VI on the abscissae of the lower panel are specified in Sec. 1. The upper and lower limits of each box represent the 75^{th} and 25^{th} percentiles, respectively; the line between these is the median value. The FM group is represented in red, NFM in gold, and NM in blue.

For the left ankle and right ankle blood flows, febrile malaria had significantly lower normalized power than NM in the 0.07-0.1 Hz and 0.8-1.4 Hz frequencies associated with the myogenic and cardiac activities respectively, and a significantly higher normalized power than NM in 0.13-0.16 Hz, the neurogenic and NO-dependent endothelial frequency intervals. A major shift was seen in the cardiac oscillatory peak between febrile malaria and non-malaria groups, with that of the febrile malaria and non-malaria found at

∼1.83 Hz, ∼1.02 Hz in the left ankle blood flow and at ∼1.8 Hz, ∼1.04 Hz in the right ankle blood flow respectively (Figure 1 (a)-(b)). As was the case for febrile malaria group, the cardiac peak frequency was slightly higher in non-febrile malaria (found at ∼1.44 Hz, ∼1.45 Hz in left ankle blood and right ankle blood flow respectively) than non-malaria. In a similar pattern to that of febrile malaria, non-febrile malaria exhibits a lower normalized power in the 0.07-0.1 Hz but was not statistically significant, and a higher normalized power around the neurogenic and NO-dependent endothelial frequency intervals all of which are statistically significant except at ∼0.02 Hz in left ankle blood flow and 0.14-0.16 Hz in right ankle blood flow, when compared to non-malaria (Figure 1(c)-(d)).

Comparisons of the normalized power between FM and NFM revealed differences in the cardiac interval, with the difference being significant only in right ankle blood flow – noting that the frequencies of their cardiac peaks also differ. At frequencies (0.04-0.05 Hz) within the neurogenic interval, NFM was found to exhibit a higher normalized power although this was only statistically significant in the right ankle blood flow (Figure 1(e)-(f)).

The box-plots in Figure 1 compare the normalised power spectral component of the LDF blood flows within the intervals investigated for different groups. The FM group was found to have lower cardiac oscillations than either the NFM or NM groups in blood flow recorded from the right ankle, and a similar significant difference in febrile malaria was observed in the left ankle blood flow cardiac band power only for the FM-NM comparison. For the respiratory interval, no significant difference was found between groups in left ankle blood flow, but respiratory normalized power in the right ankle blood flow significantly increased in non-febrile malaria only when compared with non-malaria. In contrast, values of the myogenic band power in the left ankle blood flow are less widely separated; yet they are significantly lower in febrile and non-febrile malaria groups for the FM-NM and NFM-NM comparisons, although no such significant differences were found in the right ankle blood flow. Comparisons between FM and NM revealed striking differences in the neurogenic and NO-dependent endothelial intervals, with their band powers being markedly increased in FM patients. No significant differences were found during the same comparisons for normalized band power within the NO-independent endothelial interval.

Spectral power in instantaneous heart frequency fluctuations

The IHF analysis results are summarised in Figure 2 (lower panel). Fluctuations in the IHF signal (derived from the ECG) in the frequency intervals associated with myogenic (FI-III), nitric oxide-dependent endothelial activity (FI-V) and nitric oxide-independent endothelial activity (FI-VI) ($p = 0.000006$, $p = 0.003$ and $p = 0.003$), respectively decreased significantly in febrile malaria compared to NM (Figure 2), although the spectral power around 0.021 Hz

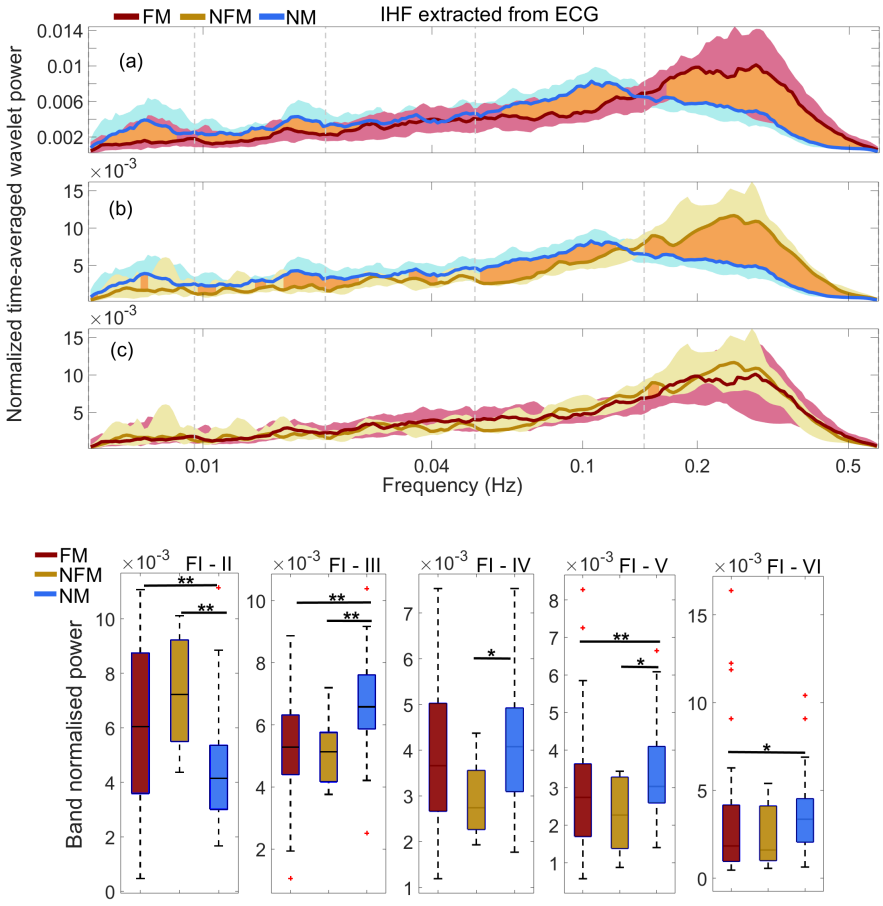

Fig. 2. Comparisons of normalised time-averaged wavelet power of the IHF extracted from ECG recordings. Each curve is obtained as a median over all subjects. (a) Febrile malaria (FM) compared with non-malaria (NM). (b) Non-febrile malaria (NFM) compared with non-malaria (NM). (c) FM compared with NFM. Red shading indicates the range between 25^{th} and 75^{th} percentiles in FM, blue shading indicates the range between 25^{th}, and 75^{th} percentiles in NM, gold shading indicates the range between 25^{th}, and 75^{th} percentiles in NFM, and brown shading indicates significant (p<0.05) differences between the FM - NM and NFM - NM comparisons. The lower panel divides the results into the six characteristic frequency intervals. The upper and lower limits of each box represent the 75^{th} and 25^{th} percentiles, respectively; the line between these is the median value. $*p < 0.05$, $**p < 0.001$. The FM group is represented in red, NFM in gold, and NM in blue. The FI-II to FI-VI frequency intervals are specified in Sec. 1.

tended to be lower for FM (Figure 2(a)). But in the FI-II frequency inter-

val associated with respiratory activity, FM exhibited a significantly higher normalised spectral power ($p = 0.0001$) compared to NM (Figure 2), similar findings was evident in the IHF absolute power (although not shown here). In a similar manner, the power of the IHF oscillations of the NFM group was significantly higher ($p = 0.004$) within the FI-II respiratory frequency interval when compared to NM, but markedly lower in the frequency intervals associated with myogenic (FI-III), neurogenic (FI-IV) and NO-related endothelial activity (FI-V) (p =0.017 and p =0.018 respectively). No significant difference was observed in any of the frequency intervals of IHF normalised spectral power in the FM and NFM comparison.

Coherence between fluctuations in IHF in left and right ankles

Figure 3 presents the averaged coherence between IHF1 and IHF2, showing that there is significant coherence in the oscillations reflecting respiratory (II), myogenic (III), neurogenic (IV) and NO-independent endothelial activity (VI), but most pronounced in the NM group, whilst within the high frequencies (> 0.1 Hz) the coherence is diminished in NFM and extremely small in FM (Figure 3(a)). The coherence in frequency intervals II, III, IV, V and VI is significantly smaller in FM ($p = 0.000000$, $p = 0.00000$, $p = 0.0000000$, $p = 0.000000$ and $p = 0.00000004$, respectively) and NFM ($p = 0.0008$, $p = 0.0005$, $p = 0.0038$, $p = 0.0021$ and $p = 0.0068$, respectively) when compared to the NM group. In the FM-NFM comparison, however, the coherence did not differ significantly in any frequency interval.

5 Non-invasive diagnosis of malaria

Detection and classification between malaria and non-malaria.

We have found that there is a set of attributes that identifies malaria efficiently, arguably providing the basis of a dynamical biomarker for malaria:

- The area under the curve showing phase coherence between the instantaneous heart frequencies (extracted from the left/right ankle LDF blood flow signals, i.e. IHF1–IHF2) in the 0.005-1 Hz frequency interval < 0.0254.
- The area under the curve showing phase coherence between the blood flow signals in the 0.6-1.6 Hz frequency interval < 0.2013.
- The area under the curve showing phase coherence between respiration and the instantaneous heart frequency in 0.145-1 Hz frequency interval extracted from the ECG < 0.0245.

Combining these characteristic attributes and using five classification algorithm from Waikato Environment for Knowledge Analysis (WEKA): J48,

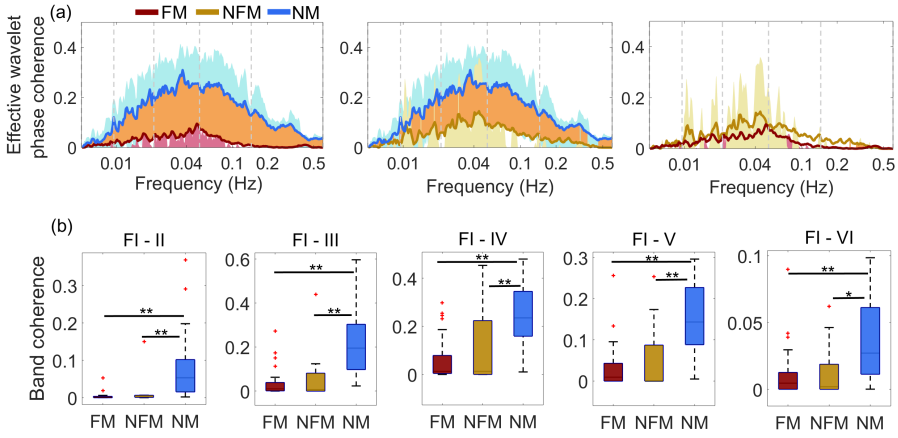

Fig. 3. Effective phase coherence: Wavelet phase coherence (minus surrogate thresholds) between IHF derived from left ankle blood flow and IHF extracted from right ankle blood flow, mean over groups, where (a) indicates comparisons between groups: the first column is the FM-NM, with NFM-NM (second column) and FM-NFM (third column). Red, blue and gold shading indicates respectively the ranges between the 25^{th} and 75^{th} percentiles for the FM, NM, and NFM groups; brown shading indicates significant (p<0.05) differences between groups. (b) Box-plots showing coherence between the IHF signals within the frequency intervals FI-II to FI-VI (see Sec. 1). $^{*}p$<0.05, $^{**}p$<0.005.

LMT, Random forest, Bagging and boosting-AdaBoos results in a high predictive performance with a classification accuracy (i.e. instances correctly classified) of 83%, 82%, 84%, 85% and 89% respectively in discriminating between FM, NFM and NM, based on the available training data (with the corresponding confusion matrix expressed in percentages in Table 2. The determining step of the diagnostic test involves detecting whether the markers are below the normal values of 0.0254, 0.2013, 0.0245 respectively for each of the markers.

Table 2. Confusion matrix, giving both the numbers and likelihoods of correct and incorrect classifications, using a Boosting algorithm.

Classified state			
Febrile malaria	Non-febrile malaria	Non-malaria	
92%	3%	5%	Febrile malaria
50%	40%	10%	Non-febrile malaria
4%	0	96%	Non-malaria
Correctly Classified Instances		87	88.7755 %
Incorrectly Classified Instances		11	11.2245 %
Total Number of Instances		98	

6 Discussion

Uncomplicated malaria presents with acute periodic episodes of fever, chills, rigors, sweating and headache. These episodes reflect infection of the RBCs by the malarial organism, its subsequent multiplication within RBCs. and later bursting of RBCs to release more organisms into blood. This cyclical process coincides with the episodes of fever. In addition the blood platelets are often affected and reduced, and abnormal adhesion of RBCs to the microvasculature results. Combined with changes in plasma, these changes lead to clogging of the microvasculature, with resulting low oxygen tension in surrounding tissues. The underlying mechanisms and pathologic processes described are unique and highly characteristic of malaria. It is probable that the physical findings observed from the study are equally specific to malaria, thereby providing an avenue for non-invasive diagnosis of malaria in the future.

Based on the hypotheses proposed above, clear distinctions have been demonstrated in the cardiovascular dynamics of subjects with febrile malaria, non-febrile malaria and healthy non-malaria, contributing to an understanding of the physiological processes occurring within the microvasculature in malaria. Furthermore, a diagnostic test has been developed based on recordings of LDF, respiration and ECG. Analyses by wavelet phase coherence and nonlinear mode decomposition enable malaria and non-malaria to be differentiated with 88 % accuracy, as classified by machine learning algorithms, based on the training data presented. Note that, we use "malaria" to describe both the febrile and non-febrile malaria patients, while "controls" or "non-malaria" are healthy subject without malaria.

As demonstrated in earlier studies on malarial microvascular function [18, 19, 45], it was observed that febrile malaria resulted in a significantly increased respiratory rate and instantaneous heart frequency, compared to healthy subjects. Skin temperature was significantly higher in malaria. Skin temperature is believed to be a determining factor of respiratory rate, and of heart rate [10]. This increase in instantaneous heart frequency alongside skin temperature in malarial subjects may perhaps result in a mixture of vasodilation, resulting in hypovolaemia, and high metabolic rate due to pyrexia. It is worth noting that a significant increase in skin temperature also leads to more vasodilation, and lowers diastolic and systolic blood pressure as observed in the malaria patients. This decrease in blood pressures of malarial patients demonstrates significant effects of the disease on both the heart's pumping function and the systemic resistance. The striking reduction in the diastolic pressure may perhaps be associated with the tachycardia observed in malaria.

Hematological examination showed a decrease of PCV in malaria. This is probably due to the compromised red blood cell deformation, and ineffective erythropoiesis within malarial vasculature [2, 42]. In terms of cardiovascular dynamics, malaria resulted in significantly reduced blood flow spectral power in the frequency interval associated with cardiac and myogenic activity. This effect is probably associated with the compromised delivery of oxygen and

nutrients observed in malaria [4, 7]. Furthermore, the lactic acidosis in the malarial state is exacerbated by inadequate removal of metabolic waste products, resulting from increased production of lactic acid by the parasites as well as reduced clearance by the liver [11].

It has also been reported that many treatments fail due to the reduced oxygen delivery in malaria, resulting in metabolic acidosis (through stimulation by cytokines), leading in turn to respiratory distress [40]. Significantly higher normalised spectral power was observed in the blood flow frequency intervals related to neurogenic (IV) and NO-dependent endothelial (V) activity in febrile malaria, compared to healthy non-malaria (Figure 1(a),(b)). However, no such effects were found in the same frequency intervals for non-febrile malaria. This might imply that these physiological processes are not markedly affected in non-febrile malaria due the absence of fever.

Coherence provides additional insight into the changes that occur with malaria in the modulation of the heart rate by the respiratory frequency. The significant attenuation of cardiac interval coherence between IHF (derived from the ECG) and breathing in malaria implies an impairment in respiratory sinus arrhythmia (RSA), given that the high frequency component in IHF reflects the influence of breathing on the heart rate [12, 21, 44], an inference that is supported by an additional finding: significantly decreased blood flow coherence in the frequency interval associated with cardiac activity. In addition, the results may also signify destruction of both the sympathetic and parasympathetic modulations that critically influence the oscillations in heart beat intervals. These modulations are widely known to contribute to the oscillatory components manifesting in IHF [6, 25, 27, 35]. Hence this finding may perhaps explain the alteration we observed in the power spectra of skin blood flow cardiac oscillations.

As mentioned above in the introduction, there are drawbacks associated with existing methods for assessing and diagnosing malaria. These have made the quest for real-time techniques for noninvasive malaria diagnosis an active area of research. Based on our findings, a cut-off was established in line with differences in cardiovascular dynamics between malarias and healthy non-malaria, with a classification accuracy of 88 % (Table 2). Early cases of non-febrile malaria, where subjects had started taking antimalarial or antipyretic drugs, were also considered as malaria in this study, due to its similarity to febrile malaria in terms of blood properties: the cytoadherence and microvasculature characteristics, including the increased stiffness of the membrane of an infected erythrocytes and their abnormal tendency to stick to endothelial cells lining the blood vessels. Consistent with this similarity, no significant differences were found in mean blood flow recorded from the extremities of the body, or in respiratory rate, between febrile malaria and non-febrile malaria. In addition, there was no significant difference in the blood flow or IHF dynamics in any of the six frequency intervals between febrile and non-febrile malaria. On the contrary, febrile malaria and non-febrile malaria differed mainly in terms of their mean skin temperature and IHF.

In summary, this study demonstrated changes in both the average values and oscillatory components of cardiovascular dynamics in malaria, in comparison with healthy non-malaria subjects, providing a better understanding of the cardiovascular physiology of malaria. A diagnostic cut-off for the early distinction between malaria and non-malaria is presented, based on differences observed in both IHF, blood flow and IHF dynamics, extracted through wavelet based analysis and nonlinear mode decomposition. Whilst this approach looks promising, as it has potential for identifying malaria noninvasively within a short period of time, future studies are needed to compare the physical findings in malaria with those in other febrile infections.

Acknowledgement. We are grateful to the participants who generously volunteered to be measured in this project. The work was supported by the Engineering and Physical Sciences Research Council (UK) Grant No. EP/M006298/1, the Tertiary Education Trust Fund (Nigeria), the Petroleum Technology Development Fund (Nigeria) under Grant No. PTDF/ED/OSS/PHD/1120/17, and the Joy Welch Educational Charitable Trust (UK).

References

1. Abdulhameed, Y.A.: Nonlinear cardiovascular oscillatory dynamics in malaria. Ph.D. thesis, Lancaster University (2020)
2. Aina, O.O., Agomo, C.O., Olukosi, Y.A., Okoh, H.I., Iwalokun, B.A., Egbuna, K.N., Orok, A.B., Ajibaye, O., Enya, V.N., Akindele, S.K., et al.: Malariometric survey of Ibeshe community in Ikorodu, Lagos state: dry season. Malar. Res. Treat. **2013** (2013)
3. Bandrivskyy, A., Bernjak, A., McClintock, P.V.E., Stefanovska, A.: Wavelet phase coherence analysis: Application to skin temperature and blood flow. Cardiovasc. Engin. **4**(1), 89–93 (2004)
4. Beards, S.C., Joynt, G.M., Lipman, J.: Hæmodynamic and oxygen transport response during exchange transfusion for severe falciparum malaria. Postgrad. Med. J. **70**(829), 801–804 (1994)
5. Bernjak, A., Cui, J., Iwase, S., Mano, T., Stefanovska, A., Eckberg, D.L.: Human sympathetic outflows to skin and muscle target organs fluctuate concordantly over a wide range of time-varying frequencies. J. Physiol. (London) **590**(2), 363–375 (2012)
6. Binkley, P.F., Nunziata, E., Haas, G.J., Nelson, S.D., Cody, R.J.: Parasympathetic withdrawal is an integral component of autonomic imbalance in congestive heart failure: demonstration in human subjects and verification in a paced canine model of ventricular failure. J. Am. Coll. Cardiol. **18**(2), 464–472 (1991)
7. Bruce-Hickman, D.: Oxygen therapy for cerebral malaria. Travel Med. Infect. Dis. **9**(5), 223–230 (2011)
8. Clemson, P.T., Lancaster, G., Stefanovska, A.: Reconstructing time-dependent dynamics. Proc. IEEE **104**(2), 223–241 (2016)
9. Clemson, P.T., Stefanovska, A.: Discerning non-autonomous dynamics. Phys. Rep. **542**(4), 297–368 (2014)

10. Davies, P., Maconochie, I.: The relationship between body temperature, heart rate and respiratory rate in children. Emerg. Med. J. **26**(9), 641–643 (2009)
11. English, M., Sauerwein, R., Waruiru, C., Mosobo, M., Obiero, J., Lowe, B., Marsh, K.: Acidosis in severe childhood malaria. QJM: Int. J. Med. **90**(4), 263–270 (1997)
12. Hinnant, J.B., Elmore-Staton, L., El-Sheikh, M.: Developmental trajectories of respiratory sinus arrhythmia and preejection period in middle childhood. Dev. Psychobiol. **53**(1), 59–68 (2011)
13. Hramov, A.E., Koronovskii, A.A., Ponomarenko, V.I., Prokhorov, M.D.: Detection of synchronization from univariate data using wavelet transform. Phys. Rev. E **75**(5), 056,207 (2007)
14. Iatsenko, D.: Nonlinear Mode Decomposition. Springer, Berlin (2015)
15. Iatsenko, D., Bernjak, A., Stankovski, T., Shiogai, Y., Owen-Lynch, P.J., Clarkson, P.B.M., McClintock, P.V.E., Stefanovska, A.: Evolution of cardiorespiratory interactions with age. Phil. Trans. R. Soc. Lond. A **371**(1997), 20110,622 (2013)
16. Iatsenko, D., McClintock, P.V.E., Stefanovska, A.: On the extraction of instantaneous frequencies from ridges in time-frequency representations of signals. Signal Proc. **125**, 290–303 (2016)
17. Iatsenko, D., Stefanovska, A., McClintock, P.V.E.: Nonlinear mode decomposition: a noise-robust, adaptive, decomposition method. Phys. Rev. E. **92**, 032,916 (2015)
18. Imai, Y., Kondo, H., Ishikawa, T., Lim, C.T., Yamaguchi, T.: Modeling of hemodynamics arising from malaria infection. J. Biomech. **43**, 1386–1393 (2010)
19. Jayathilake, P.G., Liu, G., Tan, Z., Khoo, B.C.: Numerical study on the dynamics and oxygen uptake of healthy and malaria-infected red blood cells. Adv. Appl. Math. Mech. **7**(5), 549–568 (2015)
20. Karavaev, A.S., Prokhorov, M.D., Ponomarenko, V.I., Kiselev, A.R., Gridnev, V.I., Ruban, E.I., Bezruchko, B.P.: Synchronization of low-frequency oscillations in the human cardiovascular system. Chaos **19**(3), 033,112 (2009)
21. Katona, P.G., Felix, J.: Respiratory sinus arrhythmia: noninvasive measure of parasympathetic cardiac control. J. Appl. Physiol. **39**(5), 801–805 (1975)
22. Krampa, F., Aniweh, Y., Awandare, G., Kanyong, P.: Recent progress in the development of diagnostic tests for malaria. Diagnostics **7**(3), 54 (2017)
23. Kvandal, P., Landsverk, S.A., Bernjak, A., Stefanovska, A., Kvernmo, H.D., Kirkebøen, K.A.: Low frequency oscillations of the laser Doppler perfusion signal in human skin. Microvasc. Res. **72**(3), 120–127 (2006)
24. Lancaster, G., Iatsenko, D., Pidde, A., Ticcinelli, V., Stefanovska, A.: Surrogate data for hypothesis testing of physical systems. Phys. Rep. (2018)
25. Lehtipalo, S., Winsö, O., Koskinen, L.O.D., Johansson, G., Biber, B.: Cutaneous sympathetic vasoconstrictor reflexes for the evaluation of interscalene brachial plexus block. Acta Anaesthsiol. Scand. **44**(8), 946–952 (2000)
26. Malik, M.: Heart rate variability. Ann. Noninvas. Electro. **1**(2), 151–181 (1996)
27. Meyer, M.F., Rose, C.J., Hülsmann, J.O., Schatz, H., Pfohl, M.: Impaired 0.1-Hz vasomotion assessed by laser Doppler anemometry as an early index of peripheral sympathetic neuropathy in diabetes. Microvasc. Res. **65**, 88–95 (2003)
28. Mormann, F., Lehnertz, K., David, P., Elger, C.E.: Mean phase coherence as a measure for phase synchronization and its application to the EEG of epilepsy patients. Physica D **144**(3-4), 358–369 (2000)

29. Nilsson, G.E., Tenland, T., Öberg, P.L.: Evaluation of a laser Doppler flowmeter for measurement of tissue blood flow. IEEE Trans. Biomed. Eng. **27**, 597–604 (1980)
30. Pikovsky, A., Rosenblum, M., Kurths, J.: Synchronization – A Universal Concept in Nonlinear Sciences. Cambridge University Press, Cambridge (2001)
31. Schreiber, T., Schmitz, A.: Surrogate time series. Physica D **142**(3-4), 346–382 (2000)
32. Sheppard, L.W., Stefanovska, A., McClintock, P.V.E.: Testing for time-localised coherence in bivariate data. Phys. Rev. E **85**, 046,205 (2012)
33. Sherwood, J.M., Holmes, D., Kaliviotis, E., Balabani, S.: Spatial distributions of red blood cells significantly alter local haemodynamics. PLOS ONE **9**, e100,473 (2014)
34. Shiogai, Y., Stefanovska, A., McClintock, P.V.E.: Nonlinear dynamics of cardiovascular ageing. Phys. Rep. **488**, 51–110 (2010)
35. Söderström, T., Stefanovska, A., Veber, M., Svenson, H.: Involvement of sympathetic nerve activity in skin blood flow oscillations in humans. Am. J. Physiol.: Heart. Circ. Physiol. **284**(5), H1638–H1646 (2003)
36. Stefanovska, A.: Coupled oscillators: Complex but not complicated cardiovascular and brain interactions. IEEE Eng. Med. Bio. Magazine **26**(6), 25–29 (2007)
37. Stefanovska, A., Bračič, M.: Physics of the human cardiovascular system. Contemp. Phys. **40**(1), 31–55 (1999)
38. Stefanovska, A., Bračič, M., Kvernmo, H.D.: Wavelet analysis of oscillations in the peripheral blood circulation measured by laser Doppler technique. IEEE Trans. Bio. Med. Eng. **46**(10), 1230–1239 (1999)
39. Stefanovska, A., Bračič Lotrič, M., Strle, S., Haken, H.: The cardiovascular system as coupled oscillators? Physiol. Meas. **22**(3), 535–550 (2001)
40. Taylor, T.E., Borgstein, A., Molyneux, M.E.: Acid-base status in paediatric Plasmodium falciparum malaria. QJM **86**(2), 99–109 (1993)
41. Warrell, D.A., Gilles, H.M.: Essential Malariology, 4th edn. CRC Press, London (2019)
42. Weatherall, D., Miller, L., Baruch, D., Marsh, K., Doumbo, O., Casals-Pascual, C., Roberts, D.: Malaria and the red cell. Hematology **2002**, 35–57 (2002)
43. Wilcoxon, F.: Individual comparisons by ranking methods. Biometrics Bull. **1**(6), 80–83 (1945)
44. Yasuma, F., Hayano, J.: Respiratory sinus arrhythmia – Why does the heartbeat synchronize with respiratory rhythm? CHEST **125**(2), 683–690 (2004)
45. Yeo, T.W., Lampah, D.A., Kenangalem, E., Tjitra, E., Weinberg, J.B., Granger, D.L., Price, R.N., Anstey, N.M.: Decreased endothelial nitric oxide bioavailability, impaired microvascular function, and increased tissue oxygen consumption in children with falciparum malaria. J. Infect. Dis. **210**(10), 1627–1632 (2014)
46. Yeom, E., Kang, Y.J., Lee, S.J.: Changes in velocity profile according to blood viscosity in a microchannel. Biomicrofluidics **8**, 034,110 (2014)